THE ASTROPHYSICAL JOURNAL, 325:531–543, 1988 February 15

MORPHOLOGY AND SPECTRAL CHARACTERISTICS OF THE X-RAY EMISSION OF M33

G. TRINCHIERI[1]
Osservatorio Astrofisico di Arcetri, Firenze, Italy
G. FABBIANO
Center for Astrophysics, Cambridge
AND
G. PERES
Osservatorio Astronomico, Palermo, Italy
Received 1987 May 18; accepted 1987 August 13

ABSTRACT

We have extended previous analysis of the X-ray data on M33 to include a detailed study of the morphology and spectral characteristics of its X-ray emission. In addition to the bright nuclear source and to several bright pointlike sources in the disk and arms of this galaxy, which had already been reported, we find a lower surface brightness, diffuse emission from the plane of M33. This extended emission is further separable in a hard (>2 keV) and in a soft (<1 keV) component, similarly distributed in the plane of the galaxy. We argue that the hard component is most likely the result of the integrated contribution of several lower luminosity discrete sources, similar to the ones observed in the Milky Way, e.g., compact accreting systems and young SNRs; the soft component is most likely due to the integrated emission of stellar coronae and old SNRs, although diffuse hot gas in the disk of M33 could also contribute.

The brightest source in M33 is in the nuclear region, and its average luminosity ($L_x \sim 4 \times 10^{39}$ ergs s^{-1}) is ≥ 10 times higher than the next brightest source in the plane. The nature of this source remains undetermined. The spectral results indicate a soft and intrinsically absorbed spectrum, consistent with those of low-luminosity active galactic nuclei, although the lack of signs of activity at frequencies other than the X-ray ones would make this source a unique example of "X-ray-only" activity. Alternatively the source could be explained as a new type of X-ray binary system.

Subject headings: galaxies: individual (M33) — galaxies: stellar content — galaxies: X-rays

I. INTRODUCTION

M33 is a late-type (Sc) spiral galaxy, member of the Local Group ($D = 720$ kpc; de Vaucouleurs 1978). Its proximity and face-on position in the sky have made this galaxy a very good target for detailed studies of its main components (stellar and gaseous) at several different wavelengths, from radio continuum (Berkhuijsen 1983) and radio line emission (H I; Newton 1980) to optical (de Vaucouleurs 1959, 1978) and ultraviolet (Massey and Hutchings 1983).

Long *et al.* (1981) and Markert and Rallis (1983) have reported on the X-ray observations of M33 made with the *Einstein Observatory* imaging instruments (the Imaging Proportional Counter [IPC] and the High Resolution Imager [HRI]; see Giacconi *et al.* 1979). Their analysis has revealed the presence of a number of pointlike sources in the disk and arms of the galaxy, which are mostly associated with tracers of the young stellar population. The luminosities of these sources are comparable with those of the brightest X-ray sources in the Milky Way, and range from $\leq 10^{37}$ to $\sim 10^{38}$ ergs s^{-1}. The brightest (and possibly variable) source is found at the nucleus of M33. The nature of this source is, however, not well understood (Markert and Rallis 1983) since the nucleus of M33 does not present indicators of activity at other wavelengths (O'Connell 1983; Rubin and Ford 1986).

With the exception of M31 and the Magellanic Clouds (Van Speybroeck *et al.* 1979; Long, Helfand and Grabelsky 1981; Seward and Mitchell 1981), recent work on the X-ray properties of normal, nearby galaxies has been mostly based on observations of galaxies at larger distances than M33 (see Fabbiano and Trinchieri 1987; Fabbiano 1986, 1987, and references therein). Consequently, only the brightest sources have been detected individually in these galaxies. Most of the X-ray emission appears as a diffuse source with a spatial distribution very similar to that of the optical light, possibly due to the integrated contribution of many lower luminosity ($\sim 10^{37}$–10^{38}) individual sources (see Trinchieri, Fabbiano, and Palumbo 1985; Palumbo *et al.* 1985; Fabbiano and Trinchieri 1987).

The quality and quantity of the X-ray data available for M33 together with its relatively small distance allow us to detect fainter single sources and make this galaxy an ideal target for detailed studies of the several possible components of galactic X-ray emission. The previous X-ray work had of necessity concentrated only on the resolved point sources. Our improved understanding of the characteristics of the *Einstein* instruments and the latest revision of the data analysis software allow us now to make full use of the spatial and spectral information of the entire set of *Einstein* X-ray data available for M33. Therefore we can now study the resolved bright sources with the best possible sensitivity, and we can also map the distribution of the diffuse X-ray emission. The higher spatial resolution and better sensitivity allow us to investigate the nature and spatial distribution of the diffuse disk emission at fainter intrinsic luminosities than observed in other galaxies. We can also study the spectral characteristics of the different components of the X-ray emission of M33 to further understand their nature and properties and, in particular, to set further constraints on the nature of the bright nuclear source.

[1] Also Center for Astrophysics, Cambridge.

TABLE 1

LOG OF THE OBSERVATIONS

Sequence Number	Instrument	Observation Date	Exposure Time (s)	Field Center R.A. (1950)	Field Center decl. (1950)
2090.....	IPC	1979 Aug	20745	$1^h31^m06^s.0$	30°24′00″
2724.....	HRI	1979 Aug	39085	1 31 06.0	30 24 00
2091.....	IPC	1980 Jan	13092	1 31 06.0	30 24 00
7577.....	HRI	1980 Jan	25587	1 31 26.0	30 24 22
9907.....	HRI	1980 Aug	20573	1 30 34.3	30 26 17

II. DATA ANALYSIS

M33 was observed 5 times with the instruments aboard the *Einstein Observatory*, as summarized in Table 1. For the present analysis, we have first used each image separately, in order to take into account possible time-dependent instrumental effects or significant variations in the field background from image to image. We have not found significant effects of this sort. For our morphological study of the X-ray emission of M33, we have then merged the two IPC and three HRI observations and analyzed the two resulting images in order to maximize the statistical significance of our results. As shown in Table 1, the two IPC images have the same pointing direction, therefore the merged IPC image can be analyzed as any other single *Einstein* field. Each HRI field, instead, has a different pointing direction, and therefore the three images only partially overlap. To correct for the different exposure times of each region in the merged HRI image, we have used the appropriate exposure maps.

For the spectral analysis we have used each IPC image separately, to take into account the temporal variations of the instrumental gain properly. We have also used the data from the five Monitor Proportional Counter (MPC) observations obtained simultaneously with the IPC and HRI data to gain information on the global spectral properties in a higher energy range (2–10 keV) than available with the IPC.

a) The IPC X-Ray Map

Figure 1 shows the background subtracted, isointensity contour plot of the merged IPC image, in the *Einstein* broad energy band of 0.2–3.5 keV, superposed on the optical image of the galaxy. The X-ray data have been smoothed with a Gaussian function with $\sigma = 35''$, to eliminate spurious high spatial frequencies. In order to take into account the radial dependence of the IPC background, we have used a background template by summing the two individual background maps produced by the routine reduction system (as described by Harnden *et al.* 1984). To make sure that this template reproduces correctly the background level in the image, we have compared the radial profile obtained by binning the data of each IPC field in concentric annuli about the field center with the radial profile obtained in a similar way from the corresponding background field. Since at radii $r \geq 20'$ we found a very good match between each IPC field and its corresponding background field, we are confident that the template properly represents the shape and the intensity of the field background (see also Trinchieri, Fabbiano, and Canizares 1986; Fabbiano and Trinchieri 1987). With a similar procedure, we have also produced contour plots in the soft (0.2–0.8 keV) and hard (0.8–3.5 keV) energy bands, to study the morphological differences of the X-ray emission of M33 as a function of energy. Since we did not find significant differences between the three different maps, we will refer to the broad-band map only for the rest of the paper.

As in the map in Long *et al.* (1981), the X-ray map of Figure 1 shows a dominant bright source at the galaxy's nucleus, several individual sources in the disk/arms and a source at the outskirts of the field, identified by Long *et al.* (1981) with a foreground star. Our map, however, shows more clearly the presence of a diffuse low surface brightness emission which extends over most of the optical disk of the galaxy. A quantitative discussion of this component will be given in § II*b*.

b) Radial Profiles

To study the distribution of the X-ray emission as a function of galactocentric distance we have produced radial profiles of the background subtracted surface brightness from both the merged IPC and HRI images, by binning the data in concentric annuli about the nucleus. Since we have not found significant differences in the overall shape of the distribution in the different IPC energy bands, we will discuss only the profile from the broad energy band, which maximizes the statistical significance of the data.

The azimuthally averaged profile obtained from the IPC data extends out to a radius $r = 19'$ (Fig. 2*a*). A strong, pointlike source dominates the emission for $r < 2'$. At larger radii, the profile appears rather irregular because of the many bright individual sources in the plane of the galaxy. However, most of these sources are concentrated in the western half of the galaxy (see Fig. 1), while a lower surface brightness extended component is visible mostly in the eastern half of the galactic plane. To study this component, we have produced separate profiles for the eastern and western halves of M33. These are shown in Figures 2*b* and 2*c*. While the western profile is heavily affected by the single bright sources, the eastern one is smoothly decreasing and can be followed out to $r \sim 10'$, corresponding to about one-third of the isophotal 25 mag arcsec^{-2} radius ($R_{25} = 29'$; de Vaucouleurs 1978).

We have also produced an analogous profile from the merged HRI image, shown in Figure 3. Since the instrumental background of the HRI is higher than that of the IPC and the sensitivity is lower, the HRI profile conveys less information on the low surface brightness emission than does its IPC counterpart. However, the much higher angular resolution of the HRI allows a more detailed study of the structure of the emission in the immediate neighborhood of the nuclear region. The HRI radial profile shows in fact some diffuse emission surrounding the strong pointlike source at the nucleus that can be distinguished from it at $r \sim 40''$, and extending out to $300''$.

c) Luminosities of the Different Components

The count rates of the different components of the X-ray emission associated with M33 are summarized in Table 2. The total integrated luminosity is derived from the merged IPC image by summing the net counts within a circle of 19′ radius centered on the nucleus (outside of this radius the emission is no longer detected; see Fig. 2), and subtracting the background estimated from the background map, as discussed above.

The resulting total X-ray luminosity is $\sim 1.2 \times 10^{39}$ ergs s^{-1} (for the spectral parameters of Table 2) and is due to three main components: a dominant nuclear source, several bright ($\geq 10^{37}$ ergs s^{-1} each) pointlike sources mainly on the spiral arms (see Long *et al.* 1981; Markert and Rallis 1983), and a low

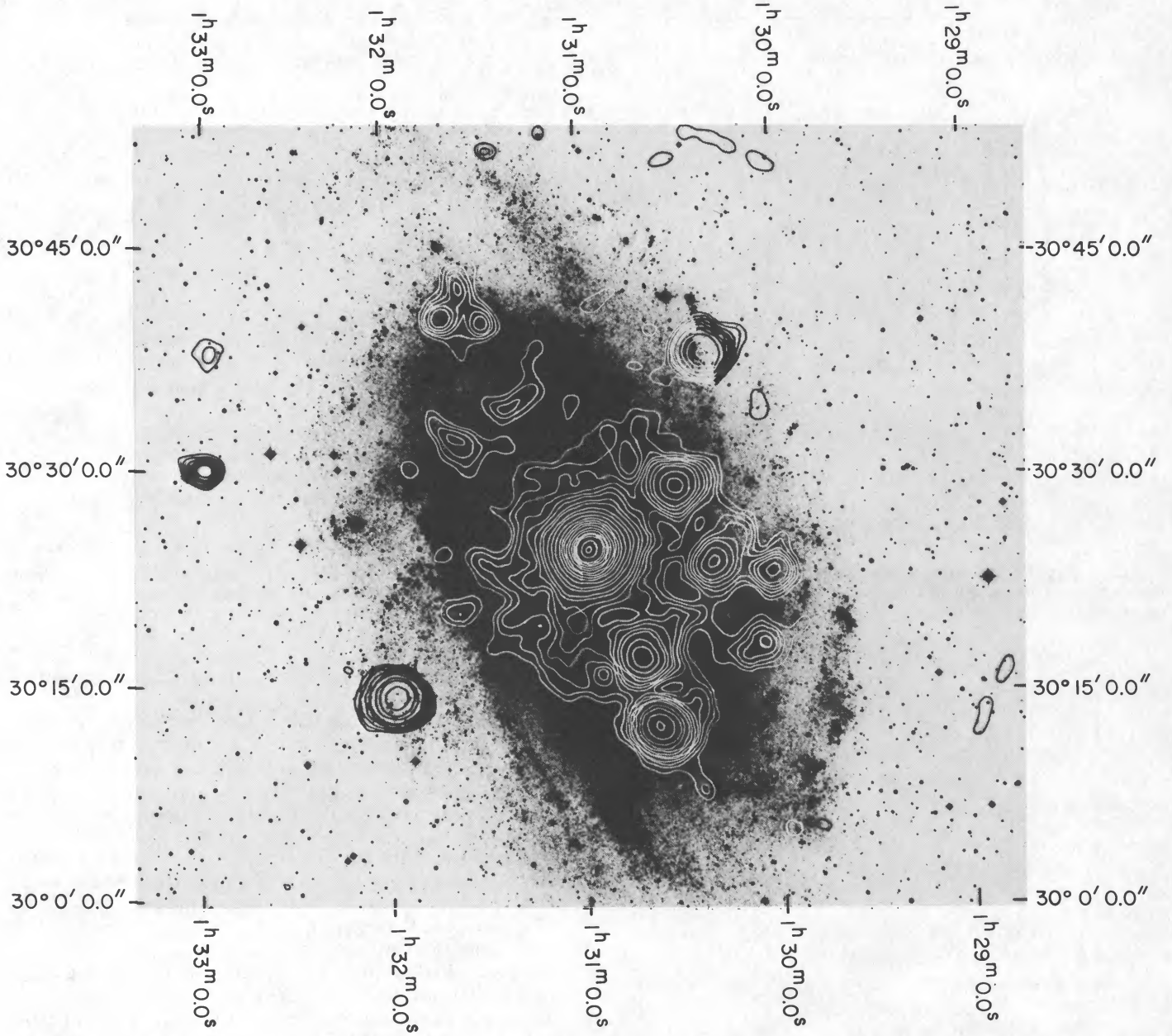

FIG. 1.—Background-subtracted, isointensity X-ray contour map (from IPC data) superposed on an optical image of M33 (from the POSS plate). The X-ray data refer to the "broad" *Einstein* energy band (0.2–3.5 keV) and have been smoothed with a Gaussian of $\sigma = 35''$.

surface brightness emission from the galactic plane. This latter component accounts for about two-thirds of the emission from the plane of M33, i.e., between 4′, to avoid the contribution from the nuclear source, and 11′, where the low surface brightness emission can no longer be detected (see Fig. 2*b*).

Although an accurate list of sources is given by Markert and Rallis (1983; see also Long *et al.* 1981), we have reanalyzed the merged IPC and HRI images to take advantage of the improved sensitivity for the detection of fainter sources allowed by the larger statistics in the merged images and the better definition of the diffuse emission in M33 and of the IPC background (see § II*b*). The results of our analysis are given in Table 3 (we use the numbering of Markert and Rallis for easy reference).

We confirm the X-ray positions and luminosities of the sources listed in Markert and Rallis (1983). In addition we detect two previously unreported sources in the merged HRI field, X-14 and X-15. We also notice that source X-9 is composed of three individual peaks (see Fig. 1). To estimate the relative contribution of each individual peak of source X-9, we cannot use the standard 3′ cell used for the other sources (see Table 3), because a circle centered on one of the peaks will include counts from the others. We have therefore obtained the counts in a circle of 5′ radius centered midway between the peaks. We have then assigned to source 9c the counts in the upper half semicircle, and to sources 9b and 9a those in the lower western and eastern quadrants, respectively. The errors given are statistical only.

d) Spectral Analysis

We have used the X-ray data from M33 to study the spectral characteristics of the four galactic components discussed above: the bright pointlike nucleus, the total nonnuclear galac-

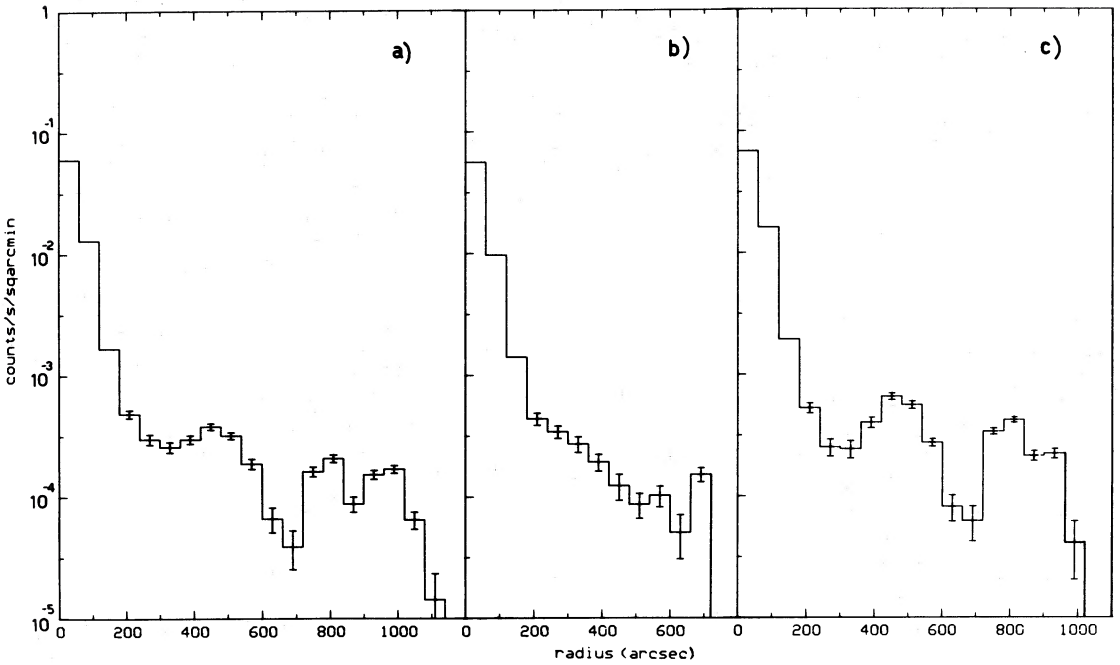

FIG. 2.—Radial surface brightness distribution of the IPC data. Data are background-subtracted and are binned in annuli of width 60″ centered on the bright nuclear X-ray source. (*a*) azimuthally averaged over 360°. (*b*) data from the left (eastern) half (0°–180° sector) only. (*c*) data from the right (western) half (180°–360° sector) only.

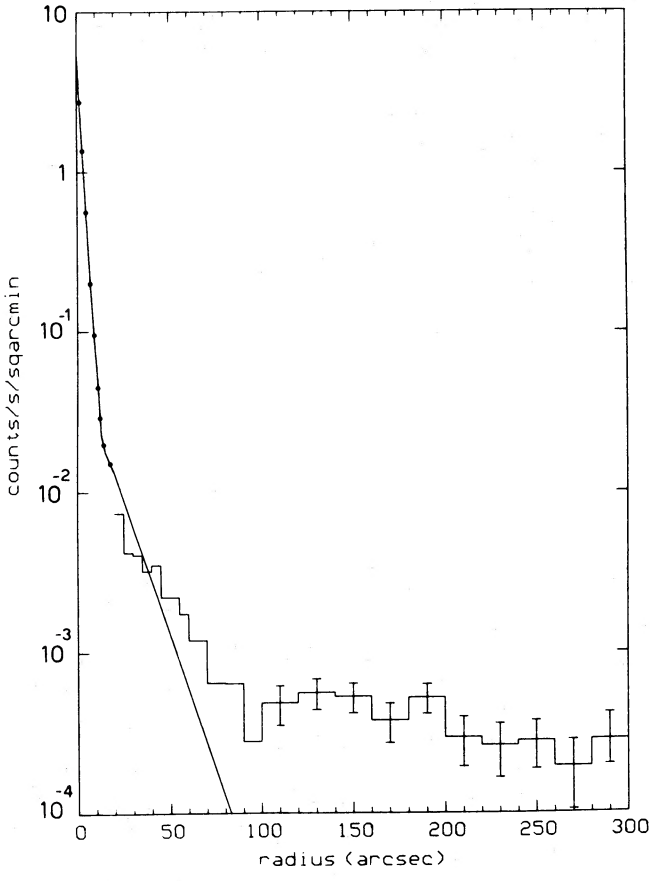

FIG. 3.—Radial surface brightness profile of the central region of M33 obtained from the HRI data, azimuthally averaged over 360°. The HRI PRF is also shown.

tic emission, the bright sources, and the extended, lower surface brightness component.

We have analyzed each IPC image separately to take into account the temporal variations of the instrumental gain. In particular, the first observation is further separated into two segments, corresponding to significantly different values of the gain (~ 12 and ~ 18). For the nuclear source data, however, the standard *Einstein* data analysis system provides an appropriate histogram of the gain variations (BAL histogram) within one observation (see Harnden *et al.* 1984), which we can use in our analysis to account for the changes in the gain.

For the spectral analysis, we have estimated the background locally from the same images. This method assures that both source and background counts were observed at the same instrumental gain and avoids the problem of possible spectral variation of the background taken at different times or positions in the sky (see also Trinchieri, Fabbiano, and Canizares 1986; Fabbiano and Trinchieri 1987). Moreover, to check that we did not significantly underestimate the background level, we have compared the net counts used in this analysis with the results obtained using the background templates. The two estimates were in agreement at $\leq 5\%$ (see also Trinchieri, Fabbiano, and Canizares 1986).

i) *Nuclear Spectrum*

The net counts used for the spectral analysis are obtained in a 3′ radius cell, and the background is estimated from the adjacent annulus of 6′ outer radius. A few sources are then included in the background region. However, the nucleus dominates the emission, and a different choice of the background does not significantly affect the results. The spectral distribution of the counts of this source observed in the 2091 image are shown in Figure 4*a*. A thermal bremsstrahlung and a power-law model with low-energy cutoff have been fit to the data. The results are given in Table 4.

TABLE 2

DIFFERENT COMPONENTS OF M33 X-RAY EMISSION[a]

Component	Inner and Outer Radii	Net Counts[b]	Error	Flux[b] (ergs cm^{-2} s^{-1})	Luminosity[c] (ergs s^{-2})
Whole galaxy	0′–19′	17395	±182	2.1×10^{-11}	1.2×10^{39}
Nonnuclear emission	4′–19′	5025	±143	5.9×10^{-12}	3.7×10^{38}
Nuclear source	0′–3′	11120	±110	1.5×10^{-11}	9.4×10^{38}
"Point sources"	...	3978	±105	6.9×10^{-12}[d]	4.3×10^{38}[d]
Extended disk component	4′–11′	~1500[e]	~84[e]	1.8×10^{-12}	1.1×10^{38}

[a] IPC data only.
[b] From the *Einstein* broad-band data (0.2–3.5 keV).
[c] Calculated in 0.2–4.0 keV band, for a thermal bremsstrahlung spectrum with $kT = 5$ keV and $N_H = 6 \times 10^{20}$ cm^{-2}.
[d] Flux and luminosity of each source is corrected for the IPC Point Response Function.
[e] Estimated from the eastern half and scaled for the total area in the ring.

The two separate images give consistent results: both models represent equally well the X-ray data, and both require a large value for the low energy cutoff. In particular, the equivalent absorbing column N_H required is much larger than the galactic value of $\sim 6 \times 10^{20}$ cm^{-2} (Stark *et al.* 1987) and also larger than the values derived from H I measurements in M33 ($\sim 10^{21}$ cm^{-2}; Newton 1980), which suggests absorption intrinsic to the nuclear region.

To increase the statistical significance of our results, we have added the two χ^2 grids obtained above. This is equivalent to considering every spectral channel for each observation as an independent point and avoids the problem of different instrumental gains, which do not allow us to perform a straightforward fit to the sum of the spectral data in different observations (see also Fabbiano and Trinchieri 1987). With this procedure, we have to assume that the source has a spectrum constant with time. However, the two separate images give both similar counting rates and consistent spectral parameters, which justify the assumption of a constant spectrum in the two observations.

The allowed parameter space resulting from this procedure is considerably reduced with respect to that obtained from the individual observations. The 90% confidence regions for the two models are plotted in Figure 4*b*, which shows that, for a bremsstrahlung model, the data require temperatures kT between ~1.0 and 5 keV, and for a power-law model, the allowed values of the energy index α range between 1 and 2. In either case, the absorption is well above the H I values.

To get an independent measure of the spectral parameters, we have also used the data from the MPC, which was observing M33 whenever either the IPC or the HRI were in the telescope focal plane. We can use the data for all five observations, albeit with some caution.

The MPC is not an imaging instrument, and it averages together all the photons that reach its field of view. It therefore will sum together photons from the nucleus and from the rest of the galaxy. However, the IPC and HRI images show that the central source dominates the emission. Moreover, the MPC response has a pyramidal shape, and therefore gives less weight to those sources not in the center of the field. Using the MPC response (see *Einstein Observatory* Revised User's Manual 1984), we have estimated that the emission from M33 that we

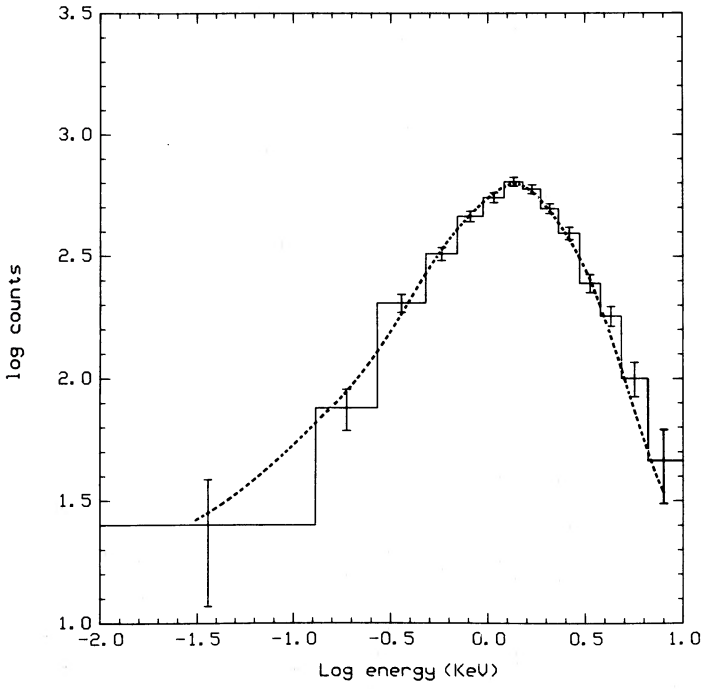

FIG. 4*a*

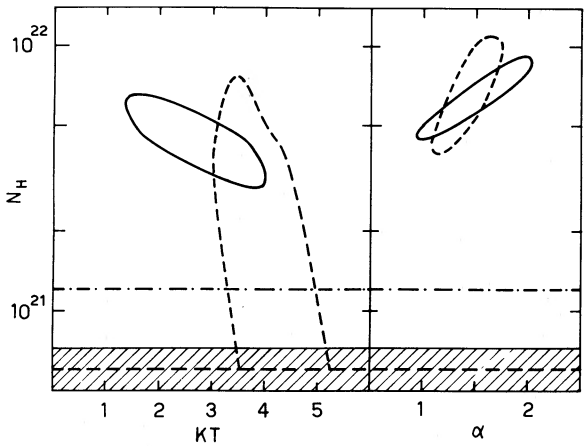

FIG. 4*b*

FIG. 4.—(*a*) Distribution of counts in the IPC energy channels for the source at the nucleus of M33. Dashed line represent the best-fit power-law model. (*b*) The 90% confidence regions in the kT-N_H and α-N_H parameter space for the source in the nuclear region of M33. *Solid contour*: results from the IPC data. *Dashed contour*: results from the MPC data. Shaded area indicates the 90% confidence region (Elvis *et al.* 1986) for the galactic N_H (*dashed line*; from Stark *et al.* 1987). Dot-dashed line indicates the N_H in the M33 nucleus (Newton 1980).

detect in the IPC outside a radius of 3′ would contribute at most 25% of the total MPC flux. Therefore, the MPC data should be dominated by the counts due to the nuclear source and give an accurate estimate of its spectral parameters. We have used the whole set of MPC data to estimate the spectral parameters of the central source. Although the pointing directions of two of the observations (H7577 and H9907) were displaced by ~4′ and ~7′ from those of the other three fields, we have estimated that this could have caused a decrease of only ~10% on the counting rate of the central source. Moreover, the counting rate in the five MPC observations was constant within the errors (see Peres *et al.* 1987).

We have fitted the same models used for the IPC analysis to the MPC data, and the results are given in Table 4. The spectral fits to each separate observation give consistent results, and χ^2 values indicate that either model can be used to represent the data. As for the IPC, we have added together the χ^2 grids. The final results are shown in Figure 4. The 90% MPC

TABLE 3

X-RAY SOURCES DETECTED IN M33

		HRI		IPC			
NUMBER	R.A. decl.	Net Counts[a]	Flux[b] Luminosity	Net Counts[c]	Flux[b] Luminosity	HARDNESS RATIOS[d]	NOTES OR IDENTIFICATION[e]
X-1	$1^h30^m04^s.28$ 30°22′54″	26.1 ±7.0	3.8×10^{-13} 2.4×10^{37}	177.1 ±29.1	1.2×10^{-13} 1.8×10^{37}	0.46 ±0.18	
X-2	$1^h30^m06^s.5$ 30°17′54″	...	...	106.4 ±26.8	1.8×10^{-13} 1.1×10^{37}	>0.37	
X-3	$1^h30^m22^s.51$ 30°23′20″	154.5 ±15.3	7.2×10^{-13} 4.5×10^{37}	156.0 ±35.5	2.3×10^{-13} 1.4×10^{37}	0.22 ±0.23	
X-4	$1^h30^m27^s.07$ 30°37′50″	...	...	652.9 ±34.0	1.2×10^{-12} 7.3×10^{37}	0.60 ±0.06	
X-5	$1^h30^m34^s.87$ 30°28′39″	109.3 ±15.5	4.4×10^{-13} 2.8×10^{37}	445.0 ±41.7	6.6×10^{-13} 4.1×10^{37}	0.65 ±0.11	
X-6	$1^h30^m40^s.35$ 30°12′11″	...	...	1040.5 ±41.5	1.7×10^{-12} 1.1×10^{38}	0.61 ±0.05	
X-14	$1^h30^m41^s.98$ 30°18′14″	52.3 ±13.5	2.1×10^{-13} 1.3×10^{37}	...	...	...	Radio source id. with SNR[f]
X-7	$1^h30^m44^s.98$ 30°16′51″	144.0 ±16.5	5.9×10^{-13} 3.7×10^{37}	469.8 ±45.2	7.0×10^{-13} 4.4×10^{37}	0.65 ±0.12	
X-8	$1^h31^m01^s.36$ 30°24′15″	4044.3 ±64.6	1.3×10^{-11} 8.1×10^{38}	11120.0 ±110.0	1.5×10^{-11} 9.4×10^{38}	0.58 ±0.01	
X-13	$1^h31^m03^s.58$ 30°17′49″	37.3 13.0	1.3×10^{-13} 8.1×10^{36}	...	...	...	
X-15	$1^h31^m12^s.53$ 30°22′55″	34.3 ±12.8	1.3×10^{-13} 8.4×10^{36}	...	...	...	~5″ from radio source 44[g]
X-12	$1^h31^m18^s.00$ 30°34′04″	115.3 ±15.6	5.2×10^{-13} 3.3×10^{37}	...	...	...	
X-9b	$1^h31^m36^s$ 30°40′00″	... ...	... ...	54.1 ±16.7	...	...	Near Hα emission[h] In spiral arm?
X-9c	$1^h31^m42^s$ 30°41′00″	...	...	53.1 ±21.6	4.0×10^{-13} 2.5×10^{37}	0.41 ±0.14	Background galaxy?[i]
X-9a	$1^h31^m48^s.2$ 30°40′11″	...	...	145.7 ±19.3	...	...	
X-10	$1^h32^m02^s.1$ 30°14′03″	...	...	947.1 ±38.8	1.7×10^{-12} 1.1×10^{38}	0.63 ±0.05	
X-11	$1^h33^m03^s.0$ 30°29′45″	...	...	132.8 ±23.0	3.2×10^{-13}	0.30 ±0.18	Not in M33

[a] Average values over three HRI observations, except for source X-1 observed only in H9907. The net counts are obtained using an 18″ circle, with the background estimated locally around it.

[b] In cgs units, calculated in 0.2–4.0 keV band, for a thermal bremsstrahlung spectrum with $kT = 5$ keV and $N_H = 6 \times 10^{20}$ cm^{-2}. Corrections for dead time, vignetting and point response function are applied.

[c] Average values over two IPC observations. The net counts are in a 3′ circle. Due to the presence of complex, extended emission, the background is estimated locally only for sources 2, 4, 10, 11. For the other sources, the background is estimated from a region at the same galactocentric distance in the eastern part of the image. For source 9, see text.

[d] Defined as the ratio between the difference in net counts in the hard (0.8–3.5 keV) and soft (0.2–0.8 keV) bands, and the net counts in the broad (0.2–3.5 keV) band. For IPC sources only.

[e] Possible identifications are only given for sources 14, 15, and 9. For a discussion of the other sources; see Long *et al.* 1981 and Markert and Rallis 1983.

[f] Viallefond *et al.* 1986.

[g] Israel and Van der Kruit 1974.

[h] Courtes *et al.* 1987.

[i] Christian and Schommer 1982.

TABLE 4

SPECTRAL ANALYSIS RESULTS FOR NUCLEAR SOURCE

Image	Count Rate Error	kT 90% Confidence Limits	N_H 90% Confidence Limits	χ^2 ν	α[a] 90% Confidence Limits	N_H 90% Confidence Limits	χ^2 ν
I2090	0.96	4.1	6.3×10^{21}	0.6	1.4	6.3×10^{20}	1.5
(MPC)	±0.07	2.3–7.3	$<1.6 \times 10^{22}$	3	0.9–2.2	$<2.5 \times 10^{22}$	3
I2090	0.3368	1.7	5×10^{21}	15.4	1.9	7×10^{21}	16
(IPC)	±0.0043	1.3–3.6	3.5×10^{21}–7×10^{21}	7	0.9–2.6	3.5×10^{21}–1×10^{22}	7
H2724	0.90	4.1	1×10^{21}	1.3	1.4	6.3×10^{21}	2.1
(MPC)	±0.07	2.2–7.3	$<1.6 \times 10^{22}$	3	0.8–2.2	$<2.5 \times 10^{22}$	3
I2091	1.08	4.6	6.3×10^{21}	1.6	1.1	1.6×10^{21}	0.9
(MPC)	±0.07	2.9–8.3	$<10^{22}$	3	0.7–1.9	$<1.6 \times 10^{22}$	3
I2091	0.3190	2.4	4×10^{21}	5.4	1.5	6×10^{21}	5.2
(IPC)	±0.0055	>1.5	2.5×10^{21}–6.5×10^{21}	8	0.8–2.5	3.5×10^{21}–8×10^{21}	8
H7577	0.86	2.6	10^{22}	0.5	1.9	1.6×10^{22}	1.7
(MPC)	±0.07	1.6–5.8	$<1.6 \times 10^{22}$	3	1.2–2.7	2.5×10^{21}–3.1×10^{22}	3
H9907	0.94	4.1	4×10^{21}	1	1.5	10^{22}	1.2
(MPC)	±0.07	2–8	$<2.5 \times 10^{22}$	3	0.8–2.5	$<4 \times 10^{22}$	3

[a] Energy exponent α is defined as $f_\nu \propto \nu^{-\alpha}$.

confidence region for the power-law model overlaps the IPC region; for a thermal spectrum, kT ranges from ~3 to 4 keV. Both models require N_H significantly larger than the H I data indicate.

A recent analysis of the spectral characteristics of the nuclear source of M33 using *Exosat* data by Gottwald, Pietsch, and Hasinger (1987) suggests, however, a somewhat different spectrum. The results from the medium-energy (ME) data, which covers an energy interval similar to the MPC band but with greater spectral resolution, are in good agreement with our results, both for the power-law and for the thermal bremsstrahlung models, and would suggest absorption higher than the line-of-sight column density observed in the 21 cm line. However, when the above authors consider the broad-band filter data from the low-energy *Exosat* detector together with the ME data they find that a simple power law no longer reproduces adequately the data, and they have to add a high-energy exponential cutoff to the model. In this case, the N_H is lowered to the line-of-sight value.

Our results from the IPC analysis alone, however, suggest a large low-energy cutoff. Since the spectral characteristics of the IPC allow a reliable measure of the column densities in the range 10^{19}–10^{22} cm^{-2} (see also Fabbiano, Trinchieri, and Van Speybroeck 1987), and since the IPC results are consistent with the MPC and ME results, we will assume an absorption in the X-ray data higher than that suggested by the 21 cm observations.

ii) *Spectrum of the Total Nonnuclear Emission*

The spectral properties of the galaxy as a whole will be completely dominated by those of the nuclear region, if we include it in the analysis. We have therefore studied the spectrum of the X-ray emission averaged over the whole galactic plane, excluding the nuclear region. The results should be more directly comparable with the average spectral properties derived for other normal spiral galaxies which do not show a prominent X-ray nucleus (see Fabbiano and Trinchieri 1987).

For this analysis we have derived the net counts with an annulus of 4′–10′, with the background estimated from that adjacent annulus of outer radius $r = 14'$. An inner radius of 4′ should ensure that the contribution from the strong central source is negligible (see Fig. 2). For the outer radius, we have confined ourselves to 10′, corresponding to the outer radius at which the extended emission is observed (Fig. 2*b*), in order to retain enough space in the IPC field for a reliable background estimation and to minimize the spatial gain variation across the field. We have used the method for analyzing extended sources that takes into account the uncertainty in the gain averaged over the appropriate area (see Fabricant and Gorenstein 1983; Trinchieri, Fabbiano, and Canizares 1986; Fabbiano and Trinchieri 1987; Fabbiano, Trinchieri, and Van Speybroeck 1987), and we have fitted a thermal bremsstrahlung spectrum with low-energy cutoff to each separate image.

The results are given in Table 5. All three images indicate that the integrated nonnuclear X-ray emission from M33 has a hard ($kT > 1$ keV) spectrum with no intrinsic low-energy absorption in addition to the galactic column density along the line of sight. If we combine the results obtained separately for each image by adding the χ^2 grids (see above), we get a tighter constraint on the temperature, with $kT \geq 3$ keV (90% confidence, see Fig. 5). The average spectral properties of M33 are therefore similar to those of other normal spiral galaxies studied (see Fabbiano and Trinchieri 1987).

iii) *Spectrum of the Bright Sources*

The net counts in each source in each separate image (or portion thereof) are in most case too few for us to attempt a meaningful spectral fitting procedure. Moreover, the sources are located outside of the calibrated region for spectral analysis of point sources (see Harnden *et al.* 1984), further complicating the study of the spectral properties of each source.

To get an indication of the spectral properties of these sources, we have done the following. First, we have calculated a hardness ratio (HR) for each source, listed in Table 3. We have found that for all sources HR is consistent with a value of ~0.6, although it might be lower for sources X-3 and X-11 (this latter is not in M33; Long *et al.* 1981). This suggests that the average spectral properties are the same for all sources in M33, and are similar to the properties of bright sources in other spiral galaxies (see Fabbiano and Trinchieri 1987). We have then performed a spectral fitting using the sum of the net counts attributable to the three sources in the 4′–10′ annulus,

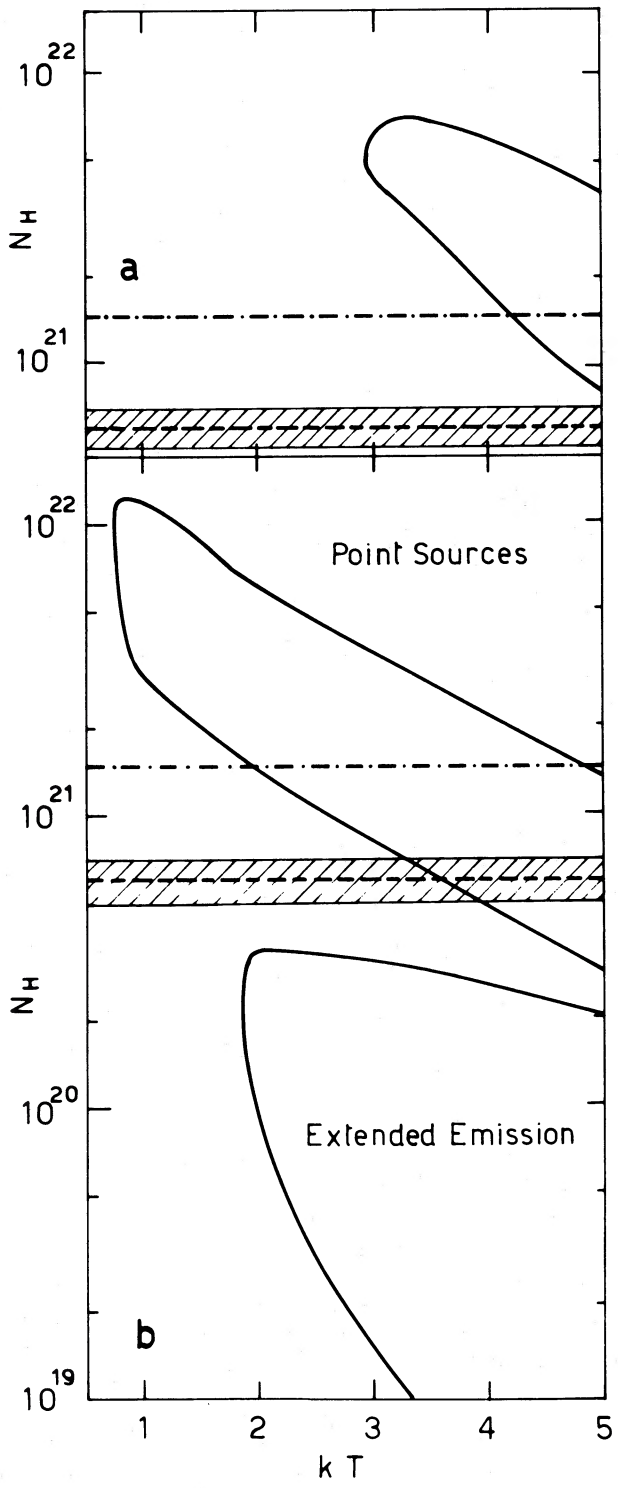

FIG. 5.—90% confidence regions in the kT-N_H parameter space for (*a*) the galactic plane, (*b*) the bright sources (*upper contour*) and the extended disk emission (*lower contour*). Shaded area indicates the 90% confidence region (Elvis *et al.* 1986) for the galactic N_H (*dashed line*; from Stark *et al.* 1987). Dot-dashed line indicates the N_H in the M33 plane (Newton 1980).

and treating the data as if they were due to an extended component. The contribution of the diffuse galactic emission is subtracted from the counts of each source by estimating the background at the same radial distance as the sources, but in the eastern half of the galactic plane.

The results of this procedure are only suggestive, because the actual number of individual sources is small (three), and the effects of spatial gain variations therefore could be severe (see Fabbiano, Trinchieri, and Van Speybroeck 1987). However, we notice that, due to the different roll angles in the two observations, the sources are located at different positions in the detector in the two IPC observations. Therefore, by repeating the analysis for the separate images, we are sampling different effects of the spatial variations of the gain. Moreover, we have repeated the analysis for one sequence (I2091) varying the fiducial value of the gain (± 1 of the nominal value determined by the use of the on-board calibration source) to estimate the effects of the uncertainty in the gain.

The results obtained at the nominal gain for each separate image are given in Table 5. The spectral parameter are not well defined, although in general they suggest a spectrum with temperatures $kT \geq 0.5$ keV. The low-energy absorption is consistent with the observed galactic column density, although some intrinsic absorption is not excluded by the fit. If we take into account the uncertainty in the gain, the results do not vary significantly from those obtained at the nominal gain. The lower boundary of kT becomes ~ 0.1 keV at the 90% confidence level (from 0.5; see Table 5), while N_H at the extremes ranges from $\geq 3 \times 10^{20}$ cm^{-2} to $\leq 10^{23}$ cm^{-2} (5×10^{20}–5×10^{22} cm^{-2} in Table 5). As for the previous components, we have summed the three separate χ^2 grids, and we show the result at the 90% confidence level in Figure 5.

iv) *Spectrum of the Extended Component*

Finally, we have studied the spectrum of the low surface brightness extended component mostly visible eastward of the nuclear source. For this purpose, we have used all the net counts in an annulus of 4′–10′, above a background estimated from the adjacent annulus extending to 14′. From this area we have excluded the regions occupied by the bright sources. We have then applied the algorithm for extended sources (as in § II*d*[ii]) to the three separate images. The results are given in Table 5. The 90% confidence contour obtained by summing the χ^2 grids is shown in Figure 5.

We find that the data can be well represented by a thermal spectrum with chracteristic temperatures $kT > 1$–1.5 keV. However, they also require a low-energy absorption well below the line-of-sight equivalent column density. This is quite different from the results obtained above for the bright sources in the plane, where we found that the range in N_H would always be consistent with, or possibly greater than, the line-of-sight column density. This result increases in significance if we combine the observations (see Fig. 5), but is already significant at greater than 90% confidence for sequence I2091 alone. To ensure that our results are not affected by a significant residual background, we have artificially increased the background counts in each spectral channel by $\sim 5\%$ to match the level expected from the background template. The results from this new set of data are totally consistent with the previous ones.

The above results are best illustrated in Figure 6, where we compare the energy distribution of the counts observed in I2091 with a thermal spectrum with $kT = 5$ keV (best fit temperature of Table 5) and the line-of-sight absorption. A spec-

TABLE 5

SPECTRAL ANALYSIS RESULTS[a]

Component	Image	Net Counts Error	kT (keV) 90% Confidence Limits	N_H (cm^{-2}) 90% Confidence Limits	χ^2_ν	Notes
Nonnuclear emission	I2090. one	890	3.1	2.4×10^{20}	4.0	1
		±62	>1.2	5.0×10^{19}–7.0×10^{20}	10	
	I2090. two	1119	5.0	2.4×10^{20}	3.5	1
		±71	>1.6	6.0×10^{19}–1.5×10^{21}	6	
	I2091	1017	5.0	2.4×10^{20}	8.2	
		±72	>2.3	8×10^{19}–1×10^{21}	8	
Bright sources	I2090. one	349	5.0	7×10^{20}	13.9	1
		±48	>0.5	1.7×10^{20}–1.5×10^{22}	10	
	I2090. two	494	1.6	2.9×10^{21}	17.5	1
		±49	>0.1	2.5×10^{20}–1.2×10^{22}	6	
	I2091	290	5.0	2.9×10^{21}	9.5	2
		±56	>0.5	5×10^{20}–5×10^{22}	8	
Disk emission	I2090. one	391	2.7	8.4×10^{19}	6.4	1
		±47	>0.5	$<8 \times 10^{20}$	10	
	I2090. two	505	5.0	8.4×10^{19}	6.3	1
		±53	>1.6	$<8 \times 10^{20}$	6	
	I2091	476	5.0	1×10^{19}	6.7	
		±55	>1.2	$<3.2 \times 10^{20}$	8	

NOTES.—(1) I2090. one: $t = 8100$ s, BAL ~ 19.4; I2090. two: $t = 12400$ s, BAL ~ 12.2. (2) Count rate is lower because source X-7 has varied (see Peres *et al.* 1987).

[a] Fitted to a bremsstrahlung spectrum with low-energy cutoff.

trum with the same temperature and no absorption is also shown. The models and the data are normalized at energies above 1 keV. For energies below 1 keV the data show a significant excess over the expected absorbed spectrum drawn as a dot-dashed curve. Since it is unlikely that the extended emission from the disk is not absorbed by the intervening neutral hydrogen, we can assume that the excess counts are due to an additional component with a much softer spectrum.

e) The Soft Component

The spectral analysis of the extended low surface brightness emission shows that this emission has a hard and a soft component. There are no significant differences in their respective distributions in the plane of the galaxy.

To estimate the relative luminosities of these two components, we have to make assumptions about their respective spectral characteristics. In particular, to estimate the X-ray

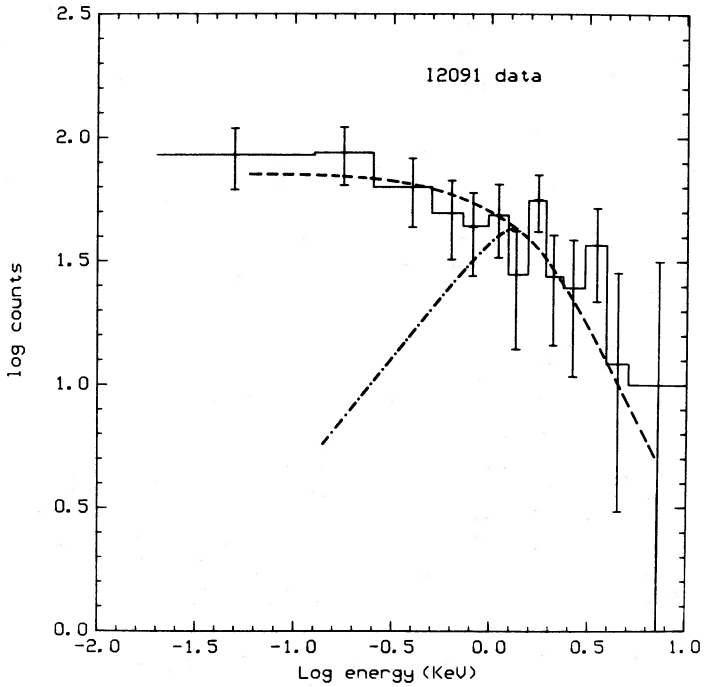

FIG. 6.—Distribution of counts in the extended disk component detected in the IPC energy channels for I2091. Dashed line represent a thermal spectrum with $kT = 5$ keV and $N_H = 1 \times 10^{19}$ cm^{-2}; dot-dashed line is for $N_H = 6 \times 10^{20}$ cm^{-2}.

TABLE 6

PARAMETER ESTIMATES FOR "SOFT" COMPONENT

HARD COMPONENT PARAMETERS		COUNT RATES	SOFT COMPONENT L_x (0.15–1.5 keV)[a]			
			$N_H = 6 \times 10^{20}$		$N_H = 10^{21}$	
			$kT = 1$	$kT = 0.2$	$kT = 1$	$kT = 0.2$
$kT = 2$	$N_H = 6 \times 10^{20}$	0.011	1.7×10^{37}	6.9×10^{37}	1.7×10^{37}	9.8×10^{37}
$kT = 2$	$N_H = 14 \times 10^{20}$	0.015	2.3×10^{37}	9.5×10^{37}	2.3×10^{37}	1.3×10^{38}
$kT = 5$	$N_H = 6 \times 10^{20}$	0.014	2.2×10^{37}	8.8×10^{37}	2.2×10^{37}	1.2×10^{38}
$kT = 5$	$N_H = 14 \times 10^{20}$	0.017	2.7×10^{37}	1.1×10^{38}	2.7×10^{37}	1.5×10^{38}

[a] Calculated assuming an optically thin thermal spectrum with solar abundances (Raymond and Smith 1977; Raymond 1980) for the parameters below kT (in keV) and N_H.

luminosity of the soft component, we have to take into account two main sources of uncertainties: the counts attributed to this soft excess and its assumed spectrum. The former depends on the other hand on the assumptions made about the spectral parameters of the hard component that is subtracted from the data.

In Table 6 we summarize the count rate and the corresponding luminosities of the soft component for different assumptions of the spectral parameters both of the hard component that is subtracted and of the soft component. The numbers in Table 6 should also be multiplied by a factor of ~ 1.4 to take into account the area masked by the bright sources. The X-ray luminosity that can be attributed to this soft component then ranges from ~ 2 to 20×10^{37} ergs s^{-1}.

III. DISCUSSION

a) *The Nuclear Source*

The brightest X-ray source in M33 is located in the nuclear region, positionally coincident (within the X-ray errors) with the optical center of the galaxy (de Vaucouleurs and Leach 1981). Markert and Rallis (1983) have extensively discussed the nature of this X-ray source. They conclude that it is probably a very low luminosity active nucleus, although they cannot rule out the possibility of a close accreting binary system.

To further investigate the nature of this source, we can examine the information contained in its X-ray spectrum. The results from the spectral analysis presented above show that the data can be represented equally well by a thermal spectrum or by a power-law model. Both models require a large equivalent column density which should be intrinsic to the X-ray source (see § II*d* and Fig. 4).

A thermal spectrum could identify this source with a binary system. However, the parameters obtained are not consistent with those of known classes of binary X-ray sources. In fact, while the temperatures are typical of low-mass binaries, both in the Milky Way (Jones 1977), and in the bulge of M31 (Fabbiano, Trinchieri, and Van Speybroeck 1987), intrinsic low-energy cutoff have been observed so far only in massive binary systems (Schreier *et al.* 1976; Becker *et al.* 1978; Swank *et al.* 1976). A large absorption in a low-mass binary could possibly arise if the source were located in a highly obscured region, which however should be very compact, since the observed H I column density in the nuclear region is well below the values required by our spectral fit (Newton 1980).

If the source is instead a low-luminosity active nucleus, the results obtained assuming a power-law model are more typical. As shown in the previous section, the power-law slope suggested by the IPC observations is steeper than the "canonical" slope $\alpha = 0.7$ found in more luminous active galactic nuclei (Mushotzky 1984). However, recent work on spectra of AGNs has shown that the canonical slope might only be the result of selection effects, and that the spectral shapes in the X-ray band are more diverse (Wilkes and Elvis 1987). In particular, the slope could be a function of the energy interval considered, and in several objects the data indicate power-law slopes ≥ 1 in the *Einstein* energy band (see Elvis 1987 for a recent review). The high absorbing column suggested by the data can also be explained in this scenario, as it is typical of the spectra of low-luminosity AGNs (Lawrence and Elvis 1982). If we correct the observed flux for the appropriate spectral parameters (see Table 4), the X-ray luminosity of this source increases to $\sim 4 \times 10^{39}$ ergs s^{-1}, which would make this the lowest luminosity active galactic nucleus yet observed.

As discussed by Markert and Rallis (1983), there is little evidence of activity at any other wavelength. The radio continuum limits (van der Kruit 1973; van der Hulst, as cited by Markert and Rallis) indicate a radio power smaller than $\sim 10^{17}$ ergs s^{-1} Hz^{-1}; the optical data indicate a relative deficiency in hydrogen line emission of at least a factor of 30 with respect to more typical active galactic nuclei (O'Connell 1983); the infrared colors are also not typical of AGNs (Gallagher, Goad, and Mould 1982; Glass 1981). Recent detailed spectra of the central region of M33 also show Hα in absorption rather than in emission in the nucleus proper of this galaxy, although they indicate the presence of [N II] emission as well (Rubin and Ford 1986). This spectrum is rather unusual compared to other galactic nuclei, but, as the authors discuss, the difference could be due to the much higher linear resolution obtained for this galaxy, which allows a much more definite separation between nucleus and inner galactic disk. If this X-ray source indicates the presence of an active nucleus in M33, this nucleus would only manifest itself in its X-ray emission, and the lack of evidence of activity at other wavelengths would make this source a rather unique example of its class.

b) *Extended Emission from the Galactic Plane*

Two-thirds of the emission from the plane of the galaxy (within 10′) are due to an extended component. The radial distribution of this component is compared with the optical (blue) profile Σ_B in Figure 7. The X-ray surface brightness Σ_x is a composite of the HRI and IPC profiles (we use only the eastern IPC profile of Fig. 2*b* to avoid the contribution from the bright point sources), and the two optical distributions

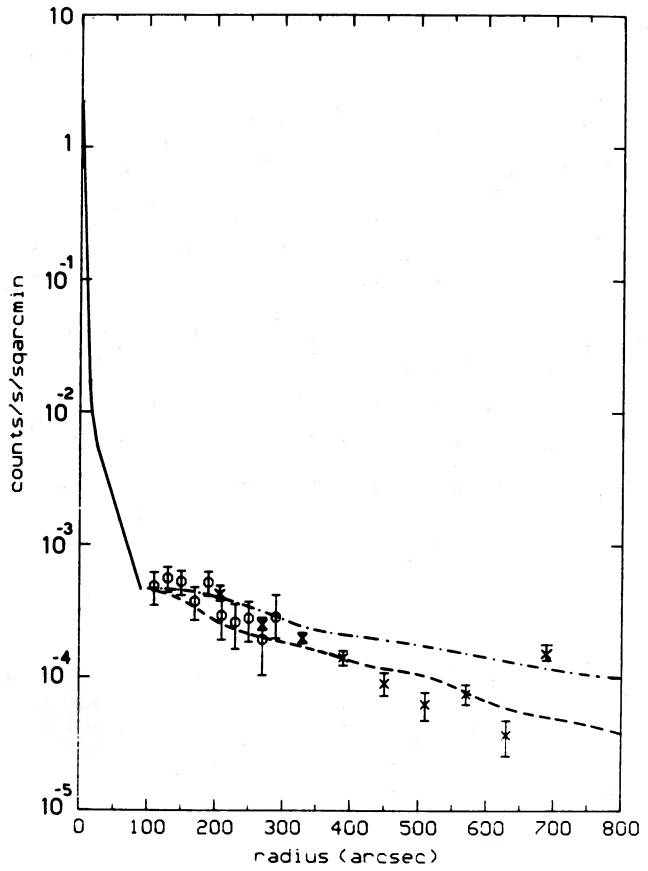

FIG. 7.—Radial distribution of the X-ray emission compared to the optical light distribution. X-ray profile is obtained from both the HRI data (*circles*), in the inner 5′, and the IPC data (eastern half only; *crosses*) from 4′ outward. The normalization between the two instruments is done in the 4′ to 5′ region. Optical data are taken from de Vaucouleurs (1959) and refer to the optical minor (*dashed line*) and major (*dot-dashed line*) axes.

refer to the major and minor axis of the galaxy (from de Vaucouleurs 1959).

As already noticed in other spiral galaxies (M83, Trinchieri, Fabbiano, and Palumbo 1985; M51, Palumbo *et al.* 1985; possibly NGC 6946, Fabbiano and Trinchieri 1987), the radial distributions of the optical and the X-ray emission are quite similar. In particular, in M33 we notice that Σ_x follows more closely the optical profile along the minor axis, except within 4′, where Σ_x seems to follow Σ_B from the major axis. This is in good agreement with the way Σ_x has been derived: for larger radii, the profile comes only from the eastern half, whose axis is close to the optical minor axis, while inside 4′, the profile is azimuthally averaged over 360°. The similarity between the X-ray and the optical blue profiles further supports the very tight link between the X-ray and the blue-emitting populations already noticed in M51 and M83 (see also Fabbiano and Trinchieri 1985) and suggests that the extended disk emission is in fact due to many lower luminosity sources that cannot be resolved individually in M33. We expect these sources to be present, by analogy with the X-ray population of our own Galaxy, the LMC and M31 (e.g., Long and Van Speybroeck 1983).

We have shown in § II that the spectrum of this component is rather peculiar, and it is most likely the sum of two components: a hard one, with spectral characteristics similar to those of the brighter, individual sources, and a luminosity L_x (0.2–4.0 keV) $\sim 10^{38}$ ergs s^{-1}, and a much softer one responsible for the excess counts in the low-energy channels, with L_x (0.15–1.5 keV) in the range ~ 2–20×10^{37} ergs s^{-1}. No significant emission is observed outside $\sim 11'$. We can, however, estimate the expected total luminosity from the disk by extrapolating the observed X-ray radial profile on the assumption that the X-ray radial distribution falls exponentially like the blue light distribution (see Fig. 7). If we assume the scale parameters for the minor axis (from de Vaucouleurs 1959), we obtain $L_x \sim 2 \times 10^{38}$ and $L_x \sim 0.4 \times 10^{38}$ ergs s^{-1} in the hard and soft components, respectively, from the 4′ to 29′ region of the disk.

The presence of a hard component is not surprising, since the vast majority of the lower luminosity sources accounting for the diffuse emission are likely to be accretion sources like white dwarf binaries and cataclysmic variables (see Hertz and Grindlay 1984) and young supernova remnants (Gorenstein and Tucker 1974), all of which have in general relatively hard spectra. Some of these sources (in particular CVs) also have a very soft component (Kylafis and Lamb 1982, and references therein). However, the large line-of-sight column density should absorb most of this soft component unless on average it has a lumonisity much larger than that of the hard component. To account for the observed excess at energies below 1 keV, we need in general an additional emitting population, with a spectrum that does not contribute significantly at harder energies.

There are two obvious sources of soft X-ray emission in galaxies: coronae of normal stars, as observed in our Galaxy (Vaiana *et al.* 1981; see also the review by Rosner, Golub, and Vaiana 1985), and a hot interstellar gas, observed in luminous elliptical galaxies (see Forman, Jones, and Tucker 1985; Trinchieri and Fabbiano 1985; Trinchieri, Fabbiano, and Canizares 1986) and predicted for spiral systems (see Bregman 1980; Corbelli and Salpeter 1987). The hot gas has been searched for in many spiral systems (M101, NGC 3628, and 4244; Bregman and Glassgold 1982; Cox and McCammon 1986; McCammon and Sanders 1984), but not detected at the expected level, although a similar feature might have been seen in NGC 4631 (Fabbiano and Trinchieri 1987). Some gaseous emission has also been observed associated with star formation activity, although in most cases it is found in star-forming regions rather than diffuse in the plane (e.g., in the nucleus of NGC 253, Fabbiano and Trinchieri 1983; η Carinae, Seward and Chlebowsky 1982). Old supernova remnants (ages 10^3–10^5 yr) also should have soft spectra and contribute to the soft excess. In all of the above cases, we expect that the spectrum should have $kT \leq 1$ keV and that the emission should be (or appear, in the case of stars) diffuse in the galactic plane.

A rough estimate of the contribution due to stellar coronae is based on the stellar content of M33 and the X-ray stellar luminosity function for our Galaxy. From the estimates of Berkhuijsen (1982, 1984) on the number of early-type stars in M33, we obtain more than 10^3 stars with mass greater than 10 $M_\odot$ in the 4′–10′ disk region. Typical X-ray luminosities of these stars are 10^{31}–10^{33} ergs s^{-1}, for a total $L_x \sim 10^{36}$ ergs s^{-1}. A greater contribution will come from low-mass, late-type stars. We estimate $\sim 10^9$ stars with mass $M \leq 1\ M_\odot$ and with $\langle L_x \rangle \sim 4 \times 10^{28}$ (Berkhuijsen 1984; Rosner *et al.* 1981; Serio 1984), which give $L_x \sim 3 \times 10^{37}$ ergs s^{-1}. Taken at face value, these numbers indicate that coronal emission of the stellar population alone could account for a large fraction, and possibly all of the soft component observed in the galactic disk. To these, we should add the emission from old supernova

remnants, which are expected (on the basis of the LMC observations; see Fusco-Femiano and Preite-Martinez 1984) to have a surface brightness too low to be detected as single sources, but which could give a significant contribution to the total emission.

Based on the previous discussion, we cannot quantify the amount of diffuse hot gas that can be present in the inner disk of M33. We have only estimated a limit on the luminosity due to this component integrated over the whole plane under the assumption that it is distributed like the disk stars, but a different distribution is certainly possible. The limits derived above of $\leq 3 \times 10^{38}$ ergs s^{-1} are comparable to the limits obtained for the edge-on spiral NGC 4244 of similar optical magnitude (Bregman and Glassgold 1982), and although significantly lower than the luminosities expected in most current models (see Bregman 1980), they could be consistent with more recent estimates from galactic fountain models (Corbelli and Salpeter 1987; see also Cox and McCammon 1986). Clearly more accurate estimates are needed for a more comprehensive understanding of the properties of a galactic hot gas component.

IV. CONCLUSIONS

The reanalysis of the X-ray data of M33 has led to two new results:

1. We have detected a low surface brightness, extended emission in the plane of the galaxy. The X-ray luminosity of this component, $L_x \sim 10^{38}$ ergs s^{-1}, is comparable to the total luminosity of the bright sources observed in the same region. Its radial distribution can be traced from $\sim 40''$ (~ 100 pc) to $\sim 10'$–$11'$ (~ 2 kpc), and is similar to the distribution of the blue light. The spectrum of this extended emission shows two distinct components: a hard one, with a temperature $kT > 2$ keV, most likely due to low-luminosity accretion sources not detected individually; and a soft one, with $kT < 1$ keV. Integrated coronal emission from the stellar population and old supernova remnants are most likely responsible for a large fraction of this component. A diffuse hot gas in the plane of the galaxy could also be contributing, although the present estimates are still too inaccurate for any further comment.

2. We have measured the spectral parameters of the nuclear source. Its X-ray spectrum can be fitted with either a low-temperature thermal emission or a steep power-law model. In both cases, a low-energy absorption intrinsic to the source is required. This spectrum is not consistent with any of the known spectra of X-ray binary sources. Although a definitive answer on the nature of this source must await future confirmation, the spectral results would favor the identification of this source with a low-luminosity active nucleus, which has an intrinsic X-ray luminosity of $\sim 4 \times 10^{39}$ ergs s^{-1}, and which is unusually quiescent at all other frequencies investigated.

G. P. acknowledges financial support by two CNR-NATO senior fellowships (No. 217.17 and 217.18), and G. T. acknowledges partial financial support from the Piano Spaziale Nazionale. G. F. thanks the Arcetri Observatory for hospitality. This work was supported in part by NASA contract NAS8-30751.

REFERENCES

Becker, R. H., *et al.* 1978, *Ap. J.*, **221**, 912.
Berkhuijsen, E. M. 1982, *Astr. Ap.*, **112**, 369.
———. 1983, *Astr. Ap.*, **127**, 395.
———. 1984, *Astr. Ap.*, **140**, 431.
Blair, W. P., Kirshner, R. P., and Winkler, P. F. 1983, *Ap. J.*, **272**, 84.
Bregman, J. N. 1980, *Ap. J.*, **237**, 681.
Bregman, J. N., and Glassgold, A. E. 1982, *Ap. J.*, **263**, 564.
Christian, C. A., and Schommer, R. A. 1982, *Ap. J. (Letters)*, **253**, L13.
Clark, G., Doxsey, R., Li, F., Jernigan, J. G., and Van Paradijs, J. 1978, *Ap. J. (Letters)*, **221**, L37.
Corbelli, E., and Salpeter, E. 1987, preprint.
Courtes, G., Petit, H., Sivan, J.-P., Dodonov, S., and Petit, M. 1987, *Astr. Ap.*, **174**, 28.
Cox, D. P., and McCannon, D. 1986, *Ap. J.*, **304**, 657.
de Vaucouleurs, G. 1959, *Ap. J.*, **130**, 728.
———. 1978, *Ap. J.*, **224**, 710.
de Vaucouleurs, G., and Leach, R. W. 1981, *Pub. A.S.P.*, **93**, 190.
Elvis, M. 1987, in *George Mason Workshop on Astrophysics, Supermassive Black Holes*, ed. M. Kafatos (Cambridge: Cambridge University Press), in press.
Elvis, M., Schreier, E. J., Tonry, J., Davis, M., and Huchra, J. P. 1981, *Ap. J.*, **246**, 20.
Elvis, M., *et al.* 1986, *Ap. J.*, **310**, 291.
Fabbiano, G. 1986, *Pub. A.S.P.*, **98**, 525.
———. 1987, preprint.
Fabbiano, G., and Trinchieri, G. 1983, *Ap. J. (Letters)*, **266**, L5.
———. 1985, *Ap. J.*, **296**, 430.
———. 1987, *Ap. J.*, **315**, 46.
Fabbiano, G., Trinchieri, G., and Van Speybroeck, L. S. 1987, *Ap. J.*, **316**, 127.
Fabricant, D., and Gorenstein, P. 1983, *Ap. J.*, **267**, 535.
Forman, W., Jones, C., and Tucker, W. 1985, *Ap. J.*, **293**, 102.
Fusco-Femiano, R., and Preite-Martinez, A. 1984, *Ap. J.*, **281**, 593.
Gallagher, J. S., Goad, J. W., and Mould, J. R. 1982, *Ap. J.*, **263**, 101.
Giacconi, R. *et al.* 1979, *Ap. J.*, **304**, 657.
Glass, I. S. 1981, *M.N.R.A.S.*, **197**, 1067.
Gorenstein, P., and Tucker, W. H. 1974, in *X-Ray Astronomy*, ed. R. Giacconi and H. Gursky (Dordrecht: Reidel), p. 267.
Gottwald, M., Pietsch, W., and Hasinger, G. 1987, *Astr. Ap.*, **175**, 45.
Harnden, F. R., Fabricant, D. G., Morris, D. E., and Schwarz, J. 1984, Scientific Specification of the Data Analysis System for the *Einstein Observatory* (*HEAO-2*) IPC, Internal SAO Spec. Rpt. No. 393.
Harris, D. E., ed. 1984, *Einstein Observatory* Revised User's Manual, Internal SAO Spec. Rept.
Hertz, P., and Grindlay, J. E. 1984, *Ap. J.* **278**, 137.
Israel, F. P., and Van der Kruit, P. C. 1974, *Astr Ap.*, **363**, 32.
Jones, C. 1977, *Ap. J.*, **214**, 856.
Kylafis, N. D., and Lamb, D. Q. 1982, *Ap. J. Suppl.*, **48**, 239.
Lawrence, A., and Elvis, M. 1982, *Ap. J.*, **256**, 410.
Long, K. S., D'Odorico, S., Charles, P. A., and Dopita, M. A. 1981, *Ap. J. (Letters)*, **246**, L61.
Long, K. S., Helfand, D. J., and Grabelsky, D. A. 1981, *Ap. J.*, **248**, 925.
Long, K. S., and Van Speybroeck, L. V. 1983, in *Accretion Driven X-Ray Sources*, ed. W. Lewin and E. P. J. van den Heuvel (Cambridge: Cambridge University Press), p. 41.
Markert, T. H., and Rallis, A. D. 1983, *Ap. J.*, **275**, 571.
Massey, P., and Hutchings, J. B. 1983, *Ap. J.*, **275**, 578.
Mathewson, D. S., Ford, V. L., Dopita, M. A., Tuohy, I. R., Long, K. S., and Helfand, D. J. 1983, *Ap. J. Suppl.*, **51**, 345.
McCammon, D., and Sanders, W. T. 1984, *Ap. J.*, **287**, 167.
Mushotzky, R. F. 1984, in *X-Ray and UV Emission from Active Galactic Nuclei*, ed. W. Brinkmann and J. Trumper (Garching-bei-Munchen: MPE Report 184), p. 73.
Newton, K. 1980, *M.N.R.A.S.*, **190**, 689.
O'Connell, R. 1983, *Ap. J.*, **267**, 80.
Palumbo, G. G. C., Fabbiano, G., Fransson, C., and Trinchieri, G. 1985, *Ap. J.*, **298**, 259.
Peres, G., *et al.* 1987, in preparation.
Raymond, J. C. 1980, private communication.
Raymond, J. C., and Smith, B. W. 1977, *Ap. J. Suppl.*, **35**, 419.
Rosner, R., *et al.* 1981, *Ap. J. (Letters)*, **249**, L5.
Rosner, R., Golub, L., and Vaiana, G. S. 1985, *Ann. Rev. Astr. Ap.*, **23**, 413.
Rubin, V., and Ford, V. L. 1986, *Ap. J. (Letters)*, **305**, L35.
Schreier, E. J., Swartz, K., Giacconi, R., Fabbiano, G., and Morris, J. 1976, *Ap. J.*, **204**, 539.
Serio, S. 1984, in *X-Ray Astronomy '84*, ed. M. Oda and R. Giacconi (Tokyo: Institute of Space and Astronautical Science), p. 1.
Seward, F. D., and Chlebowsky, T. 1982, *Ap. J.*, **256**, 530.
Seward, F., and Mitchell, M. 1981, *Ap. J.*, **243**, 736.
Stark, A. A., Heiles, C., Bally, J., and Linke, R. 1987, in preparation.
Swank, J. H., *et al.* 1976, *Ap. J. (Letters)*, **209**, L57.
Trinchieri, G., and Fabbiano, G. 1985, *Ap. J.*, **296**, 447.
Trinchieri, G., Fabbiano, G., and Canizares, C. R. 1986, *Ap. J.*, **310**, 637.

Trinchieri, G., Fabbiano, G., and Palumbo, G. G. C. 1985, *Ap. J.*, **290**, 96.
Vaiana, G. S., *et al.* 1981, *Ap. J.*, **245**, 163.
van den Heuvel, E. P. J. 1980, in *X-Ray Astronomy*, ed. R. Giacconi and G. Setti (Dordrecht: Reidel), p. 119.
van der Kruit, P. 1973, *Astr. Ap.*, **29**, 231.
Van Speybroeck, L., Epstein, A., Forman, W., Giacconi, R., Jones, C., Liller, W., and Smarr, L. 1979, *Ap. J. (Letters)*, **234**, L45.
Viallefond, F., Goss, W. M., Van der Hulst, J. M., and Crane, P. C. 1986, *Astr. Ap. Suppl.*, **64**, 237.
Wilkes, B., and Elvis, M. 1987, preprint.

G. FABBIANO: High Energy Division, Center for Astrophysics, 60 Garden Street, Cambridge, MA 02138

G. PERES: Osservatorio Astronomico, Palazzo dei Normanni, Palermo, Italy

G. TRINCHIERI: Osservatorio Astrofisico di Arcetri, Largo E. Fermi 5, I 50125 Firenze, Italy